PCCP

Accepted Manuscript

ROYAL SOCIETY OF CHEMISTRY

www.rsc.org/pccp

Strain-induced phase transition of a C_{58} solid

L. Yang,[1] H. Y. He,[1,*] J. Hu[3], B. C. Pan[1,2]
[1] *Department of Physics, University of Science and Technology of China, Hefei 230026, China*
[2] *Hefei National Laboratory for Physical Sciences at Microscale, University of Science and Technology of China, Hefei, Anhui 230026, China* [3] *Department of Physics and Astronomy, University of California, Irvine, 92697-4575, USA*

Four kinds of C_{58}-based carbon solids and some of their physical properties are predicted by the first principles calculations. These carbon solids display different electronic structures, due to their different space symmetries and connecting patterns. Among these solids, the most stable one with P3m1 space group displays semiconducting properties, with a direct band gap of about 0.12 eV, being consistent with solid C_{58} films achieved in experiment. Interestingly, this carbon solid exhibits a semiconducting-metallic phase transition under the applied uniaxial strain. The mechanism underlying such a phase transition is addressed.

PACS numbers: 61.50.Lt, 71.20.-b, 71.15.Nc, 63.20.-e, 64.60.-i

I. INTRODUCTION

Fullerenes smaller than C_{60} unavoidably possess adjacent pentagons, which increase the steric strain of the cages and make them much more chemically reactive than C_{60} [1]. Through functionalizing those active pentagon abutments, many carbon fullerene derivatives, such as exohedral fullerenes [2–5], endohedral fullerenes[6], heterofullerenes[7, 8] and even fullerene nanofilms[9, 10] have been successfully achieved in experiment. These derivatives possess catalytic properties and useful optical properties[8], and may serve as good electron-acceptors with possible photonic/photovoltaic applications[11].

On the theoretical side, carbon solids composed of different size of fullerenes were predicted, even including the smaller carbon unit C4 [12, 13]. It was found that the properties of fullenere solids were correlated with the size of the fullerene units [14–17]. Generally, fullerene solids consisting of larger fulleneres have smaller band gaps. As the size of the fullerene units decreases, the band gaps of fullerene solids increase [15]. Moreover, the solids consisting of small fullerenes exhibited superconducting features under particular conditions [18–20], due to the large electron-phonon coupling [18]. However, most studies on fullerene solids have mainly focused on those with small fullerenes, especially on the solids composed of C_{20}-C_{40} [14–20]. It has been revealed that carbon solids consisting of the fullerenes smaller than C_{60} crystallize through chemical bonds between neighboring fullerene cages, while those composed of C_{60} or larger ones through van der Waals force [21]. C_{58} fullerenes, just smaller than C_{60}, also have chemical active sites, due to existence of adjacent pentagons. Thus weak chemical bonds between neighboring C_{58} fullerenes are expected in C_{58} solids. With weak chemical bonds, solids consisting of C_{58} may display different mechanical and electronic properties from those composed of smaller fullerenes via strong chemical bonds, as well as from those with C_{60} via van der Waals interaction. Actually, solid C_{58} films have been experimentally deposited onto highly oriented phrolytic graphite in ultra high vacuum by soft-landing [22, 23]. It was found that the C_{58} films exhibited much higher thermal stability than the C_{60} solid phase and unique electronic properties [23]. Unfortunately, theoretical study on C_{58}-based solids is still lacking up to now to the best of our knowledge.

In this paper, four kinds of carbon solids are proposed from the C_{58} isomer with C_{3v} symmetry which was predicted as the most stable one among C_{58} isomers[24]. The stabilities and electronic properties of these solids are systematically investigated, on the basis of the first principles calculations. In particular, many properties including the vibrational features and the Raman spectra of the most stable one of these solids are investigated. More interestingly, this solid exhibits semiconducting-metallic phase transition under the applied uniaxial strains.

II. COMPUTATIONAL DETAILS

The density functional theory (DFT) with spin-polarized generalized gradient approximation (GGA) implemented in the SIESTA package[25–27] is employed for all the calculations. The exchange-correlation functional in the Perdew-Burke-Ernzerhof (PBE) form is adopted[28]. Norm-conserving pseudopotentials generated by using the Troullier-Martins scheme[29] are employed to describe the electron-ion interaction and the double-ζ basis sets are used for C atom. We choose unit cells consisting of two, three and four C_{58} fullerenes for constructing four different solids respectively. Accordingly, the Brillouin zone is sampled by using the Monkhorst-Pack scheme[30] with different k-point sampling up to $6 \times 6 \times 8$, which are converged for our total energy calculations. The periodic conditions are applied and the

*Author to whom correspondence should be addressed. Electronic mail:hyhe@ustc.edu.cn.

lattice constants, as well as the atom positions are fully relaxed until the Hellmann-Feynman force on each atom is smaller than 0.01 $eV/\AA$ in the calculations.

III. RESULTS AND DISCUSSION

A. Structural models of C_{58} solids

To figure out the most possible way(s) to build a C_{58} solid, we first explore the electronic features of the most stable C_{58} isomer which has the C_{3v} symmetry, as shown in Fig. 1(a). The spin moment of this C_{58} isomer is 2.0 μ_b, in good agreement with that reported in the literature [24]. In general, the activity of C_{58} fullerene molecule is governed by the molecular orbitals with their eigenvalues near Fermi level, i.e. the first two highest occupied molecular orbitals (HOMO-1 and HOMO) and the first two lowest unoccupied molecular orbitals (LUMO and LUMO+1). From the spacial distributions of their wavefunctions of these molecular orbitals as plotted in Fig. 1(b), we find that a few C atoms are more active than the others. These atoms are the so-called reactive sites where covalent bonds may form when the C_{58} solids crystallize, as depicted with red, green, violet, and yellow atoms in Fig. 1(a). As shown in Fig. 1(a), the red atom is the joint site of three hexagons(6/6/6 points); the green atoms are pentagon/pentagon adjacencies(5/5 edges); the violet atoms are pentagon/hexagon adjacencies(5/6 edges); and the yellow atoms are joint sites of pentagon/hexagon/hexagon(5/6/6 points). These adjacencies (5/5 or 5/6 edges) and joint sites are destabilizing in fullerene, and covalent functionalization these unstable sites via cycloaddition between 5/5 edges,5/6 edges or joint sites of the neighboring C58s are expected to produce stable C58 solid phase.

Based on the concerns above and the requirement of the translational symmetry in a crystal, four kinds of $C_{58}(C_{3v})$-based crystals with the space groups of P3m1, P3m1, R3m, $P6_3/mmc$[31] are proposed, the primitive unit cells of which are shown in Fig.2. Structurally, the former three belong to the Trigonal crystal system and we name them as T-I, T-II and T-III (Fig. 2(a) (b) (c)) respectively; the last one belongs to Hexagonal system and we denote it as H-I (Fig. 2(d)). In these C_{58} solids, five kinds of connecting patterns between C_{58} isomers are included, which are named as I-Bond([2+2] cycloaddition between 5/5 edges of neighboring C58 cages), II-Bond(single bond between 5/6/6 points of neighboring C58 cages), III-Bond([2+2] cycloaddition between 5/6 edges of neighboring C58 cages), IV-Bond([2+2] cycloaddition between 5/5 and 5/6 edges of neighboring C58 cages) and V-Bond(single bond between 6/6/6 points of neighboring cages) respectively, as inserted in Fig. 2.

The optimized lattice parameters, the mass densities and the bulk moduli of the C_{58} solids are summarized in Table-I. As listed in Table-I, T-II and T-III have very similar lattice parameters and hence have the same mass density. With the covalent inter-cage bonds, the bulk moduli ranging from 36.6 to 76.2 GPa of these C_{58} solids are much bigger than that (less than 0.01 GPa) of C_{60} molecular solids, but much smaller than that (436.1 GPa) of the diamond [15]. The mass density of our proposed C58 solids ranges between 1.08 and 1.59 g/cm^3, of which the C_{58} cages in both T-II and T-III are more closely packed. These density is much smaller than that of diamond(3.52 g/cm^3), but comparable to that of the polymeric phases of C60 (about 1.80 g/cm^3, from the reported volume per mole) achieved in experiments [32, 33]. Moreover, due to the different connecting patterns, these solids exhibit different magnetic and electronic properties: the former three possess magnetism, while the latter does not; the former is semiconducting with a finite band gap of 0.12 eV, while the latter three are metallic.

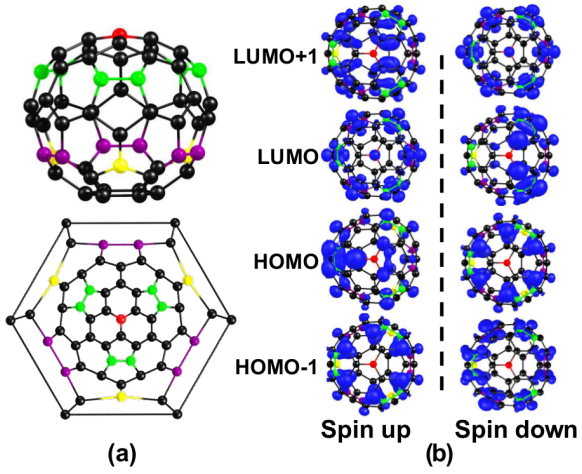

FIG. 1: (a)Geometry (upper panel) and Schlegel diagram (lower panel) of C_{58} fullerene with C_{3v} symmetry; (b)the charge density distribution of the energy levels near the fermi level of the isolated C_{3v}-C_{58} isomer.

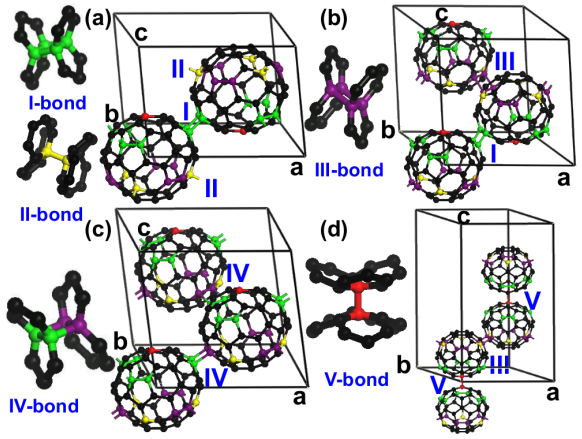

FIG. 2: The primitive unit cells for (a)T-I, (b)T-II, (c)T-III and (d)H-I. The inserts are the five different connecting patterns between C_{58} isomers: I-Bond, II-Bond, III-Bond, IV-Bond and V-Bond.

The narrow band gap of the T-I structure is consistent with the ultraviolet spectra prediction of narrow gap for C_{58} films [23].

B. Structural stabilities of C_{58} solids

We then concern the structural stabilities of the C_{58} solids, which can be determined by the formation energy defined as[17]

$$E_f = (E_{solid} - n * E_{cage})/n, \quad (1)$$

where E_{solid} and E_{cage} are the total energies of the C_{58} solid and the fullerene molecule, respectively, and n is the number of C_{58} cages in a primitive unit cell. The calculated formation energies of all C_{58} solids are listed in Table I. It can be seen that T-I has much lower formation energy than the others, thus this structure may be the ground state of C_{58} solid. Such big difference of the formation energies is important to obtain pure phase and high quality of C_{58} solid. Furthermore, we find the formation of the C_{58} solid in the T-I structure is an exothermic process, while that in T-II, T-III or H-1 is an endothermic one. We thus infer that the supposed T-I C_{58} solid may have similar structure to that of the C_{58} film achieved in experiment [22, 23]. Therefore, we focus on the T-I C_{58} solid in the below.

To examine the dynamic stability of T-I structure, we calculate its phonon spectrum, of which the phonon dispersion at low frequency below 400 cm^{-1} is displayed in Fig. 3(a). Clearly, there is no imaginary mode shown in the phonon spectrum. This strongly confirms that the C_{58} solid with T-I structure is dynamically stable, so it is a new metastable configuration in the carbon family. The corresponding vibrational density of states (VDOS) is shown in Fig. 3(b), in which the local VDOS for the bridging atoms(B-atoms) between the cages is illustrated. From the Fig. 3(b), we can see the B-atoms vibrational modes mainly position at the frequencies between 800 and 1200 cm^{-1}. Checking the vibrational features, we find that the peak at about 850 cm^{-1} mostly corresponds to the translation modes of the B-atoms between the cages, and the peaks at 1000-1200 cm^{-1} are associated to the mixing features of torsional vibrations of the B-atoms.

We further calculate the intensity of Raman active modes of T-I, by using the empirical bond polarizability model[34, 35]. The calculations are performed at the phonon temperature of 300 K, with a laser excitation wavelength of 514.5 nm. To test our implementation of this method, we first calculated the Raman shift of the diamond, from which our calculated Raman shift of 1294.6 cm^{-1} is close to the value of 1333.0 cm^{-1} measured in the experiment [36]. This demonstrates the reliability of our used method. The calculated Raman spectrum for T-I is plotted in Fig. 4(a), in which the Raman spectra of the isolated C_{58} is included for comparison. From Fig. 4(a), one can see that two striking peaks present at 482.6

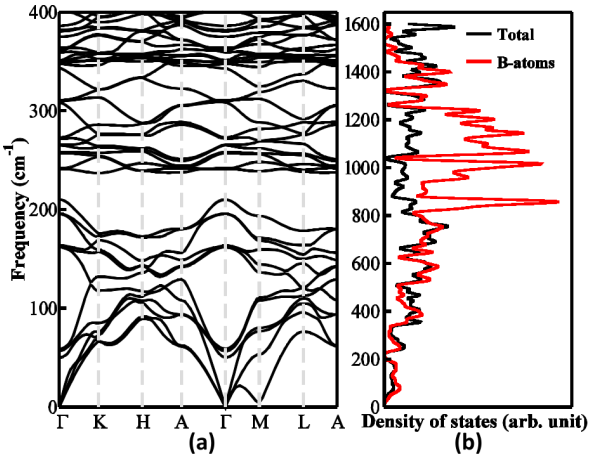

FIG. 3: (a)The phonon dispersion for the frequency below 400 cm^{-1} and (b) the vibrational density of states for T-I and the bridging atoms(B-atoms).

and 1527.9 cm^{-1} in the Raman spectrum of the isolated C_{58} isomer, corresponding to the pentagon breathing mode and the stretching mode of the C=C bonds. These characteristic Raman features of the isolated C_{58} isomer still remain in the Raman spectrum of the C_{58} solid of T-I, which position at 498.2 and 1526.8 cm^{-1} respectively, just with frequency shift of less than 16 cm^{-1}. Similar observations were reported for the Raman features of polymeric phase of C60[32], where the Raman characteristics of the pristine C60 retained in the Raman spectra of C60 polymer, and the Raman mode of C60 in high frequency (1448cm^{-1}) exhibited a redshift of 11-62 cm^{-1} for different C60 polymeric phases. Meanwhile, more Raman active modes are introduced in the Raman spectrum of T-I, due to the fact that assembling reduces the symmetry of the concerned C_{58}. Five typical peaks with relative strong intensities appear at the frequencies of 342.9, 386.0, 792.2, 1435.8 and 1564.5 cm^{-1}, which are marked with A, B, C, D and E respectively in Fig.4 (a). The corresponding vibrational patterns for these five Raman active modes are plotted in Fig. 4(b-f), which are mainly contributed from the atoms with three-fold coordinates. In addition, two inter-cage modes with weak Raman intensities are found position at 161.8 and 162.1 cm^{-1} respectively, which corresponding to the translations of the cages.

C. Strain effect on the structural and electronic properties of the T-I C_{58} solid

It is interesting to study the responses of the structural and the electronic properties of the T-I C_{58} solid to the uniaxial strain. For this concern, the energy varying with the applied strain is shown in Fig. 5(a). From Fig. 5(a), one can see the total energy of the T-I C_{58} solid increases first under both compressive and tensile strains. With the tensile strain further increasing, the total ener-

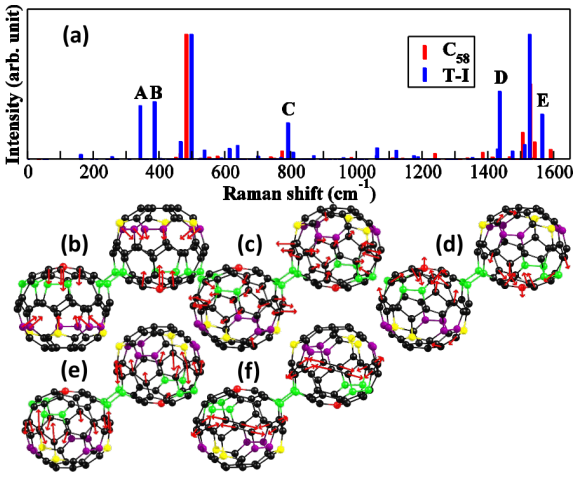

FIG. 4: (a)The Raman spectra for C_{58} isomer and T-I, (b-f)the vibrational patterns of the typical Raman active modes for T-I corresponding to the modes marked as A, B, C, D and E in (a).

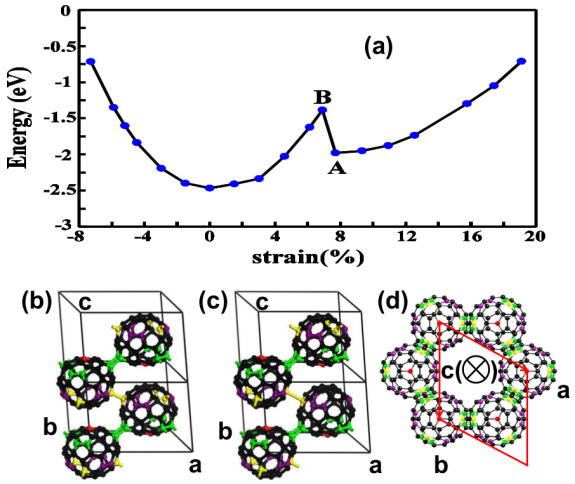

FIG. 5: (a)The energy of T-I as the function of the applied strain, and the crystal structure of T-I at (b) site B, (c) side view and (d) top view of T-I at site A. The energy of T-I in (a) takes the reference of that of the isolated C_{58}.

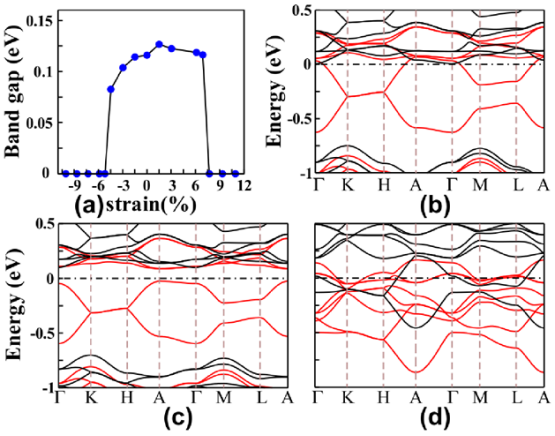

FIG. 6: (a)The band gap of T-I under strains and the band structures of T-I under (b) the compressive strain of -7.3% (c)no strain, and (d) the tensile strain of 7.7% The red lines and the black lines in (b), (c) and (d) stand for the majority and minority spin states respectively. The horizontal dot-dashed lines in (b), (c) and (d) indicate the Fermi levels, which shift to zero.

gy reaches its maximum at 6.9% and then drops abruptly to a local minimum at 7.7%, implying occurrence of a structural phase transition. Careful examination of the configuration of T-I under the strains reveals that the inter-cage bonds are elongated to some extent under the tensile strain. At the equilibrium site, I-bonds and II-bonds which connect neighboring C_{58}s are about 1.58 Å and 1.66 Å. Under the tensile strain of 6.9% (at site B in Fig. 5(a)), I-bonds and II-bonds are stretched to be 1.63 Å and 1.81 Å, where the crystal structure changes indistinctively, as illustrated in Fig. 5(b). Surprisingly, the further strain of about 7.7% induces the configuration of T-I convert to be the layered fullerenes at site A, with II-bonds being elongated to be 2.66 Å, significantly larger than that of the equilibrium structure (1.66 Å). The configurations of T-I at site A are shown in Fig. 5(c)(side view) and (d)(top view).

To go further, we investigate the corresponding electronic properties of T-I under the strains. At the equilibrium volume, the proposed T-I crystal is a semiconductor with a direct band gap of 0.12 eV, which is similar to most of the stable solids consisting of smaller fullerenes [14–17]. Interestingly, corresponding to the structural phase transition of T-I from the fullerene solid (site B) to the layered fullerene (site A), the system converts from its semiconducting feature to the metallic feature. Nevertheless, T-I also exhibits metallic features under the compressional strain larger than -5.2%, as shown in Fig. 6(a). Such semiconducting-metallic phase transition may have potential applications in strain-controlled switches.

To understand such strain induced semiconducting-metallic phase transition, we carefully inspect the electronic structures of T-I under different strains. From the spin-resolved band structures of T-I at the equilibrium volume in Fig. 6(c), we can see that the conduction band minima (CBM) of both the majority spin and the minority spin channels are very close, but the valence band maximum (VBM) of the majority spin channel is much higher than that of the minority spin channel. Therefore, the E_g in the minority spin channel (0.83 eV) is much larger than that in the majority spin channel(0.12 eV), and the E_g of the T-I C_{58} solid is determined by the majority spin channel. The band structures under strains of -7.3% and $+7.7\%$ are plotted in Fig. 6(b) and (d). For the compressive strain of -7.3% in Fig. 6(b), the dispersions of the bands are similar with that of the equilibrium case (Fig. 6(c)), but the valence bands of the majority spin channels cross the Fermi level and overlap with the conduction bands, which results in metallic

feature. On the contrary, the band structures change significantly under tensile strain of +7.7%, with the bands of both majority spin and minority spin channels cross the Fermi level, featuring a metallic character.

The calculated projected density of states(PDOS) reveal that both the majority spin and the minority spin states near the Fermi level of T-I are mainly from the contribution of p orbits of the inter-cage atoms of the neighboring C58 cages. The semiconductor-metal transition can be rationalized as below: under the compressive strain, the inter-cage bonds are shortened, and the strained bonds make the valence bands of the majority spin states move up and the conduction bands of the minority spin states move down. With the strain of −5.2% (the inter-cage bonds of I-bonds and II-bonds are compressed by about −1.9% and −3.6% respectively), the valence band and the conduction band overlap, resulting the metalization of the system. Under the tensile stain, the interactions between inter-cage bonds become weak. As the tensile strain reaches +7.7%, the configuration of T-I converts to the layered C58s hexagonal lattice. Consequently, the weak interaction between the layers metallizes the system.

IV. SUMMARY

Four kinds of C_{58} solids are predicted, on the basis of the first-principles calculations. Their stabilities, mass density, bulk moduli, magnetic and electronic properties are investigated. Of these proposed solids, the most stable one (T-I) is semiconducting with a direct narrow band gap, being consistent with the solid C_{58} films deposited in experiment. Raman analysis of T-I reveal that the characteristic Raman active modes of the isolated C_{58} isomer still retain in Raman spectra of this solid. In addition, T-I exhibits semiconductor-metal transition under the applied strain.

V. ACKNOWLEDGEMENTS

This work is supported by the National Science Foundation of China (Grant No. NSFC11105140, 11275191). The HP-LHPC of USTC is acknowledged for computational support.

[1] X. Lu and Z. F. Chen, Chem. Rev. 2005, **105**, 3643.
[2] M. Bertau, F. Wahl, A. Weiler, K. Scheumann, J. Worth, M. Keller, H. Prinzbach, Tetrahedron 1997 **53**, 10029 ().
[3] A. Koshio, M. Inakuma, T. Sugai, H. Shinohara, J. Am. Chem. Soc 2000 **122**, 398.
[4] S. Y. Xie, F. Gao, X. Lu, R. B. Huang, C. R. Wang, X. Zhang, M. L. Liu, S. L. Deng, L. S. Zheng, Science 2004 **304**, 699.
[5] P. A. Troshin, A. G. Avent, A. D. Darwish, N. Martsinovich, A. K. Abdul-Sada, J. M. Street, R. Taylor, Science 2005 **309**, 278.
[6] T. Guo, M. D. Diener, Y. Chai, M. J. Alford, R. E. Haufler, S. M. McClure, T. Ohno, J. H. Weaver, G. E. Scuseria, R. E. Smalley, Science 1992 **257**, 1661.
[7] T. Guo, C. M. Jin, R. E. Smalley, J. Phys. Chem. 1991 **95**, 4948.
[8] D. E. Clemmer, J. M. Hunter, K. B. Shelimov, M. F. Jarrold, Nature 1994 **372**, 248.
[9] D. Löffler, S. S. Jester, P. Weis, A. Böttcher, and M. M. Kappes, J. Chem. Phys. 2006 **124**, 054705.
[10] D. Löffler, S. Ulas, S. S. Jester, P. Weis, A. Böttcher and M. M. Kappes, Phys. Chem. Chem. Phys. 2010 **12**, 10671.
[11] D. L. Chen, W. Q. Tian, J. K. Feng, C. C. Sun, J. Phys. Chem. B 2007 **111**, 5167.
[12] X. L. Sheng, Q. B. Yan, F. Ye, Q. R. Zheng, G. Su, Phys. Rev. Lett. 2011 **106**, 155703.
[13] L. Yang, H. Y. He, B. C. Pan, J. Chem. Phys. 2013 **138**, 024502.
[14] S. Okada, Y. Miyamoto, and M. Saito, Phys. Rev.B 2001 **64**, 245405.
[15] G. Seifert, A. N. Enyashin, and T. Heine, Phys. Rev. B 2005 **72**, 012102.
[16] J. C. Grossman, S. G. Louie, and M. L. Cohen, Phys. Rev. B 1999 **60**, R6941.
[17] A. N. Enyashin and A. L. Ivanovskii, Phys. Rev. B 2008 **77**, 113402.
[18] Y. Miyamoto, and M. Saito, Phys. Rev.B 2001 **63**, 161401.
[19] N. A. Romero, J. Kim, and R. M. Martin, Phys. Rev.B 2004 **70**, 140504.
[20] M. Côté, J. C. Grossman, M. L. Cohen, and S. G. Louie, Phys. Rev. Lett. 1998 **81**, 697.
[21] W. I. F. David, R. M. Ibberson, T. J. S. Dennis, J. P. Hare, K. Prassides, Europhys. Lett. 1992 **18**, 219.
[22] A. Böttcher, P. Weis, A. Bihlmeier and M. M. Kappes, Phys. Chem. Chem. Phys. 2004 **6**, 5213.
[23] A. Böttcher, P. Weis, S. S. Jester, D. Löffler, A. Bihlmeier, W. Klopper and M. M. Kappes, Phys. Chem. Chem. Phys. 2005 **7**, 2816.
[24] D. L. Chen, W. Q. Tian, J. K. Feng, and C. C. Sun, ChemPhysChem 2007 **8**, 1029.
[25] P. Ordejón, E. Artacho and J. M. Soler, Phys. Rev. B 1996 **53**, R10441.
[26] D. Sánchez-Portal, P. Ordejón, E. Artacho and J. M. Soler, Int. J. Quantum Chem. 1997 **65**, 453.
[27] J. M. Soler, E. Artacho, J. D. Gale, A. García, J. Junquera, P. Ordejón. and D. Sánchez-Portal, J. Phys.: Condens. Matter 2002 **14**, 2745.
[28] J. P. Perdew, K. Burke, and M. Ernzerhof, Phys. Rev. Lett. 1996 **77**, 3865.
[29] N. Troullier and J. L. Martins, Phys. Rev. B: Condens. Matter 1991 **43**, 1993.
[30] H. J. Monkhorst, J. D. Pack, Phys. Rev. B 1976 **13**, 5188.
[31] International Tables for X-ray Crystallography Volume 1 Symmetry Groups(The Kynoch, Birmingham, England, 1952).
[32] Davydov,V. A.; Kashevarova, L. S.; Rakhmanina, A. V.;

Senyavin,V. M.; Ceolin, R.; Szwarc, H.; Allouchi, H.; and Agafonov, V. Phys. Rev. B **2000**, 61, 11936.

[33] Korobov, M. V.; Bogachev, A. G.; Popov, A. A.;Senyavin, V. M.; Stukalin, E. B.; Dzyabchenko, A. V.; Davydov, V. A.; Kashevarova, L. S.; Rakhmanina, A. V.; Agafonov, V. Carbon **2004**, 43, 954.

[34] R. Saito, T. Takeya, T. Kimura, G. Dresselhaus, and M. S. Dresselhaus, Phys. Rev. B 1998 **57**, 4145.

[35] S. Guha, J. Menendez, J. B. Page, and G. B. Adams, Phys. Rev. B 1996 **53**, 13106.

[36] M. A. Washington and H. Z. Cummins, Phys. Rev. B 1977 **15**, 5840.

TABLE I: The calculated lattice parameters a (Å) and c(Å), mass density ρ (g/cm^3), the formation energy E_f (eV), the bulk modulus B (GPa), manget per cell ($1.0\mu_B$) and band gap E_g (eV) for the four solids.

Solids	a(Å)	c(Å)	ρ(g/cm^3)	E_f (eV)	B(GPa)	magnet/cell($1.0\mu_B$)	E
T-I	13.99	9.30	1.47	-1.233	55.6	2.0	
T-II	14.16	12.58	1.59	-0.054	76.2	4.0	
T-III	14.17	12.56	1.59	0.025	75.8	6.0	
H-I	12.25	24.25	1.08	0.250	36.6	0.0	